Dynamics of quantum-classical differences for chaotic systems

L. E. Ballentine
Physics Department, Simon Fraser University, Burnaby, British Columbia, Canada V5A 1S6
(Received 25 October 2001; published 19 June 2002)

The differences between quantum and classical dynamics can be studied through the moments and correlations of the position and momentum variables in corresponding quantum and classical statistical states. In chaotic states the quantum-classical differences grow exponentially with an exponent that exceeds the classical Lyapunov exponent. It is shown analytically that the quantum-classical differences scale as $\hbar^2$, and that the exponent for the growth of these differences is independent of $\hbar$. The quantum-classical difference exponent is studied for two quartic potential models, and the results are compared with previous work on the Hénon-Heiles model.

DOI: 10.1103/PhysRevA.65.062110 PACS number(s): 03.65.Sq, 05.45.Mt

I. INTRODUCTION

In studying classical and quantum chaos, it is important to understand the evolution of the differences between quantum and classical dynamics. Two qualitatively different regimes of quantum-classical correspondence must be distinguished [1]: (a) the Ehrenfest regime, in which the centroid of the wave packet approximately follows a classical trajectory; and (b) the Liouville regime, in which the quantum probability distributions are in approximate agreement with those of a classical ensemble satisfying Liouville's equation. The limits of these regimes define two distinct quantum-classical ''break times,'' whose magnitudes and scaling properties can be quite different [2]. The Ehrenfest regime persists only as long as the width of the quantum state is small compared to the length scale of the potential, whereas the Liouville regime can persist for very wide states, for which Ehrenfest's theorem is irrelevant [1–6].

A useful way to characterize the quantum-classical differences is through the moments of the classical and quantum probability distributions for the position and momentum variables. These moments satisfy a hierarchy of equations, which may be truncated and solved numerically, provided the widths of the probability distributions remain small enough [7]. By choosing the initial quantum and classical probabilities to be equal, one can study how the differences between the quantum and classical theories grow in time, how they depend on the parameters of the initial state, and how they scale with $\hbar$. These calculations have been carried out for the Hénon-Heiles model [8], leading to several conclusions [7,9].

(i) The deviation from Ehrenfest's theorem, that is, the difference between the motion of the centroid of a quantum wave packet and a classical trajectory with the same initial condition, is not a valid measure of quantum effects. It is governed primarily by the width of the initial state, and does not scale with $\hbar$.

(ii) A true measure of quantum effects is given by the differences between the probability distributions of a quantum state and of a classical ensemble that is constructed to have the same initial position and momentum distributions. The magnitude of these differences scales as $\hbar^2$.

(iii) For chaotic states, the quantum-classical differences grow exponentially, on average, but with an exponent λ_{qc} that is larger than the classical Lyapunov exponent.

(iv) The exponent λ_{qc} is independent of $\hbar$.

Of course, the exponential growth of quantum-classical differences cannot persist indefinitely. The exponent λ_{qc} is calculated as a phase-space average of *local, short-time* Lyapunov exponents, whose computation was described in Ref. [9].

The conclusions (i)–(iv) were first demonstrated numerically for a single model, although (i) is now well established [1–6]. It is the purpose of this paper to present results for some other models, and to show how some of the conclusions can be understood from a theoretical analysis. Since the hierarchy of equations for the moments converges only for sufficiently narrow wave packets, our calculations are confined to the Ehrenfest regime. However, some results outside of this regime are discussed in the final section.

II. THEORY

The equations of motion for the moments of the probability distributions were developed in Ref. [7] for any system with two degrees of freedom and a potential that is a polynomial of the coordinates. They are sufficiently complicated that it is practical to treat them in detail only with the help of a computer algebra system such as MAPLE, from which FORTRAN code can then be obtained for subsequent numerical investigations. However, they possess a form that makes some degree of general theoretical analysis possible.

The classical equations of motion have the standard Hamiltonian form

$$\frac{dq_i}{dt} = \frac{\partial H}{\partial p_i},$$

$$\frac{dp_i}{dt} = -\frac{\partial H}{\partial q_i} \quad (i=1,2). \tag{1}$$

When the Hamiltonian H is expressed as a polynomial, the quantum-mechanical Heisenberg equations have the same form as Eq. (1), but with the coordinates and momenta, q_i

and p_i, becoming noncommuting operators. Choosing some initial state, we introduce the centroids, $Q_i=\langle q_i\rangle$ and $P_i=\langle p_i\rangle$, and the deviation-from-centroid variables

$$\delta q_i = q_i - \langle q_i\rangle, \quad \delta p_i = p_i - \langle p_i\rangle. \tag{2}$$

Here the average bracket $\langle\cdot\rangle$ denotes either a quantum average or a classical ensemble average, according to the context. The generalized moments of the deviation variables have the form

$$\tfrac{1}{2}\langle(\delta p_i)^m(\delta q_j)^n + (\delta q_j)^n(\delta p_i)^m\rangle, \tag{3}$$

with the symmetrization being necessary only for the quantum case. The equations of motion for the centroids and the moments form a hierarchy that never terminates (except in the uninteresting case of a quadratic potential), but which can be truncated at sufficiently high order. It was found in Ref. [7] that at least all terms up to fourth order ($m+n \leqslant 4$) must be included to obtain reliable results.

For notational convenience, we define $X=(X_1,X_2,\ldots)$ to be the vector of moments that are to be included in the calculation. Thus, for example: $X_1=Q_1$, $X_4=P_2$, $X_7=\langle\delta p_1\delta q_2\rangle$, $X_{14}=\langle(\delta q_2)^2\rangle$. (Up to fourth order, X has 69 elements.) The vectors of classical and quantum moments will be denoted X^c and X^q, respectively. Their time evolutions are governed by nonlinear equations, of the form

$$\frac{dX^c}{dt} = F(X^c), \tag{4}$$

$$\frac{dX^q}{dt} = F(X^q) + G(X^q). \tag{5}$$

The quantum equation (5) differs from the classical equation (4) because of the noncommutativity of the position and momentum operators. The first term on the right-hand side of Eq. (5) has the same form as in Eq. (4); the second term $G(X^q)$ contains the commutators that arise from reordering the δq's and δp's into the standard order (2). The term $G(X^q)$ is small, being of order $\hbar^2$.

In [7] and [9] the differences between the quantum and classical theories were obtained by solving Eqs. (4) and (5) separately, and subtracting the results. This involved small differences between much larger quantities, hence it was necessary to be vigilant for round-off errors, which limited the range over which the computation could be performed. A less restricted method, whose results are presented in this paper, is to define the quantum-classical difference vector

$$Z = X^q - X^c, \tag{6}$$

and obtain its equation of motion directly. Subtracting Eq. (4) from Eq. (5) and expanding to first order in Z, we obtain

$$\frac{dZ}{dt} = F'(X^q)Z + G(X^q), \tag{7}$$

where F' is the matrix of derivatives. Written in component form, the equation becomes

$$\frac{dZ_i}{dt} = \sum_j \frac{\partial F_i}{\partial X_j} Z_j + G_i. \tag{8}$$

Since Eq. (7) is a linear inhomogeneous equation, the magnitude of the solution Z is governed by the magnitude of the driving term G. Hence $Z=O(\hbar^2)$. To the lowest order in $\hbar^2$ it makes no difference whether the right-hand side of Eq. (7) is evaluated on the quantum trajectory X^q or on the classical trajectory X^c. Therefore, for further analysis, we shall replace Eq. (7) by

$$\frac{\partial Z}{dt} = F'(X^c)Z + G(X^c), \tag{9}$$

which is equivalent to the lowest order in Z, and has the advantage that all quantum effects are contained in the functional form of G.

We can now give a general proof of the properties (ii) and (iv), which were previously discovered only numerically. The inhomogeneous driving term G in Eq. (9) is generally of order $\hbar^2$. In fact, in our computations G is proportional to $\hbar^2$, although terms of order $\hbar^4$ and higher would arise if we were to include moments of sufficiently high order. (Those, however, were found in [7] to have negligible effect.) This explains why the differences Z between the quantum and classical moments scale as $\hbar^2$. Moreover, since the driving term G is proportional to $\hbar^2$, it follows that the solution $Z(t)$ is also proportional to $\hbar^2$, with its functional form being otherwise unaffected by $\hbar$. Therefore the exponent λ_{qc} that describes the growth of quantum-classical differences will be independent of $\hbar$.

The remaining qualitative result (iii), that λ_{qc} is greater than the largest classical Lyapunov exponent, is not so easy to explain. Consider the homogeneous equation related to Eq. (9),

$$\frac{dZ}{dt} = F'(X^c)Z. \tag{10}$$

Since it describes the tangent map [10] of the nonlinear equation (4), its solutions will yield the Lyapunov exponents of Eq. (4). These are not the same as the Lyapunov exponents of the classical equation of motion (1), but they are closely related. For example, the largest Lyapunov exponent of Eq. (1), λ, describes the exponential separation of two initially close classical trajectories in phase space. But the quantity $\langle(\delta q)^2\rangle$, which is an element of X^c, describes the mean-square separation of an ensemble of classical trajectories. Therefore its exponential growth rate will be 2λ, and this growth rate could also be computed from Eq. (10). Thus we see that the solutions of Eq. (10) would yield exponents that are directly related to the classical Lyapunov exponents of Eq. (1). Now in [7] and [9] it was found that $\lambda_{qc} > 2\lambda$. This larger value of λ_{qc} can only be due to the inhomogeneous term G in Eq. (9). But we have been unable to discover any useful mathematical theorems concerning the growth rates of related inhomogeneous and homogeneous equations such as Eqs. (9) and (10). Nor can we identify any

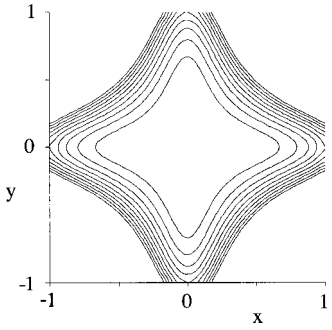

FIG. 1. Contours of the quartic potential $V(x,y)=x^4+y^4+32x^2y^2$.

of the many terms of $G(X^c)$ as being dominant. So the empirical result, $\lambda_{qc}>2\lambda$, does not yet have a general explanation.

III. RESULTS

The above theory has been applied to models whose Hamiltonians have the form

$$H=\tfrac{1}{2}(p_x^2+p_y^2)+V(x,y), \tag{11}$$

where (x,y,p_x,p_y) are alternative notations for (q_1,q_2,p_1,p_2). The initial quantum state is chosen to be a narrow Gaussian whose centroid can be located at any desired place in phase space. The initial classical state is a Gaussian probability density in phase space, constructed so that its position and momentum probability distributions agree with the quantum state. (See Ref. [7] for technical details.) A dynamic state is characterized by its centroid in configuration space, $\vec{\mathbf{Q}}=(\langle q_1\rangle,\langle q_2\rangle)$, and the sum of the variances of the two position coordinates, $V=\langle(\delta q_1)^2+(\delta q_2)^2\rangle$. The differences of these quantities between the quantum state and the classical ensemble, $|\vec{\mathbf{Q}}_q-\vec{\mathbf{Q}}_c|$ and $|V_q-V_c|$, are the principle objects of interest.

If these differences are computed by direct subtraction they are subject to round-off errors, which limited the range over which the computations could be carried out in [7]. Indeed, it was not possible to study $|\vec{\mathbf{Q}}_q-\vec{\mathbf{Q}}_c|$ over an adequate range using that method. This limitation is overcome by using the linearized Eq. (9) to compute the differences directly. We have, however, verified that the previously published results for the Hénon-Heiles model [7] were accurate. Further calculations have been carried out for two other models.

A. Quartic potential

The potential for this model is

$$V(x,y)=x^4+y^4+gx^2y^2. \tag{12}$$

Since V is a homogeneous quartic polynomial, the motions are similar at all energies, and so only the energy $E=1$ need be considered. The shapes of the equipotential curves are controlled by the parameter g. This model is separable for certain values of g (including $g=0$, 2, and 6), but is nonintegrable for most values. The value $g=32$ (see the contour diagram in Fig. 1) was chosen because a Poincaré section shows that the orbits ergodically fill most of the energetically accessible phase space. There are a few stable periodic orbits, but the regular islands around them are very small.

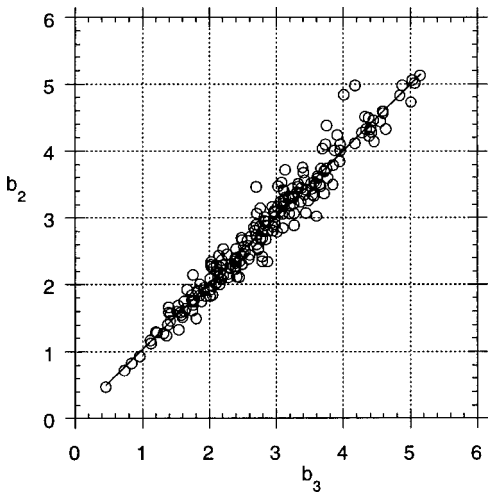

FIG. 2. Linear regression of the index b_3, for exponential growth of the difference between the centroids of the quantum and classical probabilities, vs the index b_2, for the difference between the quantum and classical variances, for the quartic potential of Fig. 1.

For chaotic states, the various moments (3) and their quantum-classical differences (6) are oscillatory with upper envelopes that grow approximately exponentially. As was described in [9], these envelopes can be fitted to exponentials: the quantum variance V_q is fitted to $e^{b_1 t}$; the difference between the quantum and classical variances $|V_q-V_c|$ is fitted to $e^{b_2 t}$; and the difference between the quantum and classical centroids $|\vec{\mathbf{Q}}_q-\vec{\mathbf{Q}}_c|$ is fitted to $e^{b_3 t}$. The exponents b_1, b_2, and b_3 are analogous to short-time Lyapunov exponents, and their values depend on the starting point of the trajectory in phase space. We expect the average of b_1 over the ergodic portion of phase space to correspond to 2λ, where λ is the largest classical Lyapunov exponent. The averages of b_2 and of b_3 define the quantum-classical difference exponent, λ_{qc},

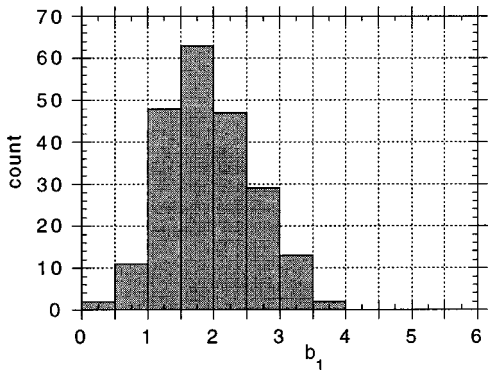

FIG. 3. Histogram of the exponent b_1 for the growth of the quantum variance, for the quartic model of Fig. 1.

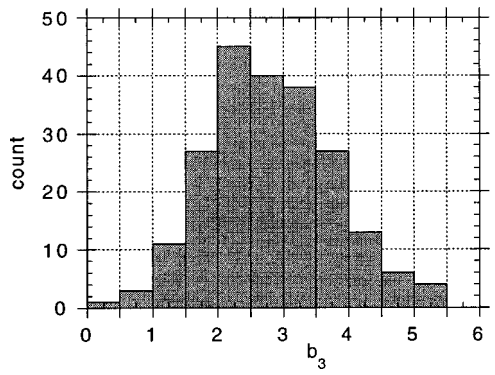

FIG. 4. Histogram of the quantum-classical difference exponent b_3, for the quartic model.

which measures the rate of separation of the quantum and classical theories.

Although there is no *a priori* reason why the averages of b_2 and b_3 must be equal, the numerical data strongly indicate that they yield the same value for λ_{qc}. Figure 2 shows that b_2 and b_3 cluster around the line $b_2=b_3$, with no evidence of any systematic differences. The slope of the best fitting straight line is 0.992, which is not significantly different from 1. This indicates that the quantum-classical differences of the centroids and of the variances grow at the same rate, and so b_2 and b_3 provide the same information. The estimates of λ_{qc} from the averages of b_2 and b_3 are 2.820 and 2.805, respectively. The difference is not significant.

The histograms of b_1 and b_3 (Figs. 3 and 4) for this model have the same general shape as was found for the Hénon-Heiles model in [9]. Figure 5 shows a linear trend of b_3 vs b_1, with no apparent systematic deviations, but with a greater scatter of the points than for the Hénon-Heiles model.

Table I compares the earlier results for the Hénon-Heiles model [9] with those for the quartic model. It is notable that $(b_1)_{av}$, which should theoretically be comparable to 2λ, is systematically larger. This is probably due to the inhomogeneous nature of phase space. The boundary between the regions of regular and chaotic orbits is not sharp, and consists

TABLE I. Lyapunov-like exponents for the Hénon-Heiles model [9] and the quartic model.

	2λ	$(b_1)_{av}$	λ_{qc}
HH ($E=0.13$)	0.113	0.145	0.221
HH ($E=0.16$)	0.222	0.246	0.371
Quartic	1.74	1.93	2.81

of a fractal set of tori. An orbit spends part of its time near these ''sticky tori,'' accumulating very small contributions to its Lyapunov exponent, and part of its time in the ergodic sea, where it accumulates large contributions to its Lyapunov exponent. The techniques of this paper apply to ensembles of orbits, rather than to single orbits. Since we wish the ensemble to be purely chaotic (or purely regular [7]), rather than mixed, the fractal boundary region was deliberately avoided. Thus the contributions from the sticky tori were underestimated, and so $(b_1)_{av}$ comes out to be somewhat greater than 2λ.

B. x^2y^2 model

The Hamiltonian for this model is given by Eq. (11) with $V(x,y)=\frac{1}{2}x^2y^2$. Since this is also a homogeneous potential, the motions will be similar at all energies, and so we shall consider only $E=0.5$. This model attracted considerable attention because it was believed that all of its periodic orbits were unstable, but that conjecture proved to be false [11].

This model differs from the others in that its energetically accessible phase space is not compact; a particle can make arbitrarily long excursions up the valleys that center on the x and y axes. The motions in the valleys are qualitatively different from the motions in the junction around the origin (Fig. 6). Motions in the valleys are *adiabatically integrable* [12]; the rapid transverse motion can be averaged to yield an effective potential for the slow longitudinal motion, which appears smooth and regular. When the particle reaches the junction, the adiabatic approximation breaks down, and the

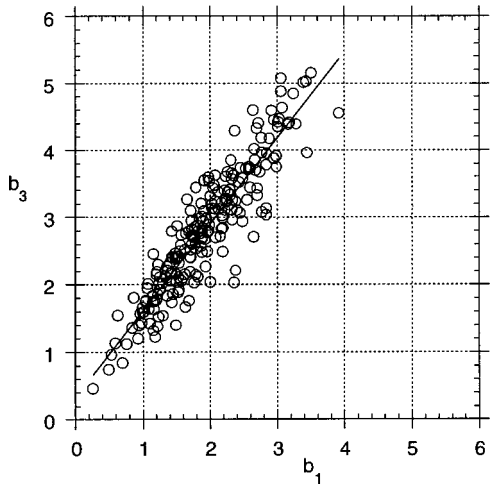

FIG. 5. Linear regression of the exponent b_3 vs b_1, for the quartic model.

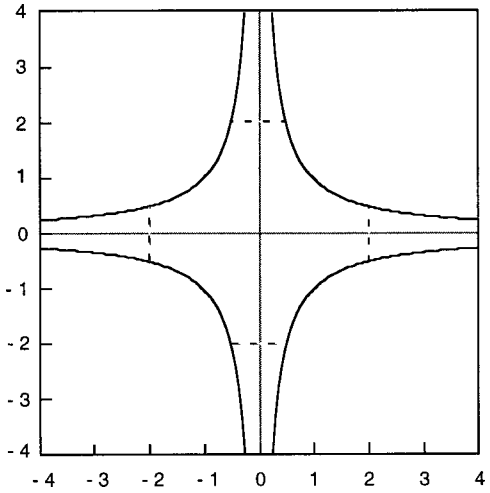

FIG. 6. Level curve $x^2y^2=1$ for the potential, showing the boundary between the valleys and the junction.

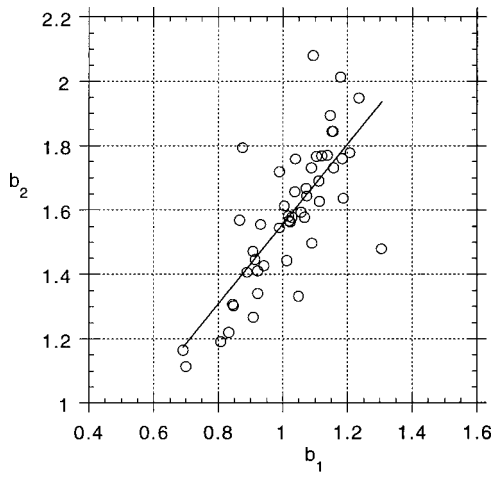

FIG. 7. Linear regression of the exponent b_2 vs b_1 for junction orbits.

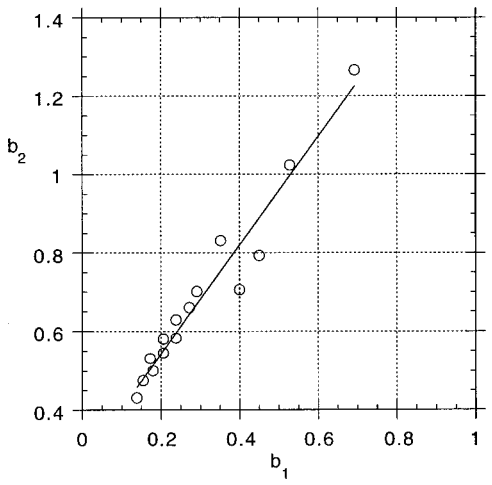

FIG. 9. Linear regression of the exponent b_2 vs b_1 for valley orbits.

motion is no longer integrable. Qualitatively, an orbit can be described as a regular motion up and down a valley, with stochastic switching between valleys as it passes through the junction. Due to the noncompact nature of the phase space and the qualitative difference between motions in the junction and in the valleys, it is not useful to compute a Lyapunov exponent, which would average over both kinds of motion.

To study the irregular junction orbits, we started orbits at a large number of initial positions and directions of motion within the junction. Many of these had to be discarded because they soon departed up a valley. The criterion was adopted that an orbit must remain within the junction (defined as $|x|$ and $|y|$ less than 2) for at least 10 time units in order to be counted. Figure 7 shows b_2 to be greater than b_1, as in the other models, but there is much more scatter about the linear regression line.

The valley orbits are quite regular, and can be studied systematically by releasing the particle at some distance $y_{\max}$ from the origin with zero longitudinal velocity, all the kinetic energy being initially confined to the transverse motion. The

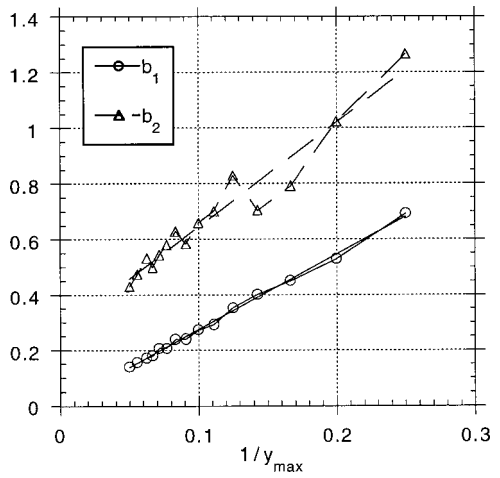

FIG. 8. Exponents b_2 and b_1 for valley orbits vs the reciprocal of the maximum extent up the valley.

long-time limit of the exponent b_1, being twice the classical Lyapunov exponent, should be zero for integrable motions. The larger the value of $y_{\max}$, the more time the orbit spends in the adiabatically integrable region, and so the smaller b_1 should be. Figure 8 shows that b_1 varies nearly linearly with $1/y_{\max}$, and does indeed approach zero as $y_{\max}$ becomes infinite. The quantum-classical difference exponent b_2 also shows an approximately linear trend with $1/y_{\max}$, but approaches a nonzero limit as $y_{\max}$ becomes infinite.

Figure 9 shows the linear trend of b_2 vs b_1. Similar results have been found for all models, and are summarized in Table II.

IV. CONCLUSIONS

A general analytic derivation has now been provided for some results that were previously only known numerically. These are that the differences between quantum and classical-ensemble dynamics scale as $\hbar^2$, and that for chaotic states the exponential growth exponent of these differences, λ_{qc}, is independent of $\hbar$. Two more models have been studied in detail, confirming the general picture that was obtained in earlier studies [7,9] of the Hénon-Heiles model. In addition, we find that the difference between the centroids of the quantum and classical probability distributions grows with the same average exponent, λ_{qc}, as does the difference between the quantum and classical variances.

The short-time exponent for the growth of quantum-classical differences (b_2) shows a linear correlation with the exponent for the growth of the mean square width of the state (b_1). The slope of the regression line of b_2 vs b_1 (see

TABLE II. Linear regression of b_2 vs b_1.

HH ($E=0.13$)	$b_2=0.017+1.412b_1$
HH ($E=0.16$)	$b_2=0.037+1.356b_1$
Quartic	$b_2=0.228+1.346b_1$
x^2y^2 (junction)	$b_2=0.316+1.241b_1$
x^2y^2 (valley)	$b_2=0.265+1.384b_1$

Table II) is dimensionless, and so can be meaningfully compared between models. That its value (about 1.35 on average) is always greater than 1, is related to the previously known fact that $\lambda_{qc} > 2\lambda$, since the two sides of the inequality are identified with the averages of b_2 and b_1, respectively. These two interesting facts have yet to find a general theoretical explanation. Recently, however, this qualitative behavior has been confirmed on a very different system (interacting spins) by a different technique (direct integration of the equations of motion) [2], so there is reason to believe that it is typical.

Another interesting question is the time over which the exponential growth of the quantum-classical differences persists. Our computations with the moment equations are necessarily restricted to the Ehrenfest regime (narrow states). However, the results of [2] suggest that this exponential growth does not persist outside of the Ehrenfest regime, and that the quantum-classical differences have a different behavior in the broader Liouville regime.

ACKNOWLEDGMENT

This work was supported by a grant from the Natural Sciences and Engineering Research Council of Canada.

[1] L. E. Ballentine, Y. Yang, and J. Zibin, Phys. Rev. A **50**, 2854 (1994).
[2] J. Emerson and L. E. Ballentine, Phys. Rev. A **63**, 052103 (2001).
[3] L. E. Ballentine, Phys. Rev. A **47**, 2592 (1993).
[4] K. Takahashi and A. Shudo, J. Phys. Soc. Jpn. **62**, 2612 (1993).
[5] B. S. Helmkamp and D. A. Browne, Phys. Rev. E **49**, 1831 (1994).
[6] J. Emerson and L. E. Ballentine, Phys. Rev. E **64**, 026217 (2001).
[7] L. E. Ballentine and S. M. McRae, Phys. Rev. A **58**, 1799 (1998).
[8] M. Hénon and C. Heiles, Astron. J. **69**, 73 (1964).
[9] L. E. Ballentine, Phys. Rev. A **63**, 024101 (2001).
[10] A. J. Lichtenberg and M. A. Lieberman, *Regular and Chaotic Dynamics* (Springer, New York, 1992).
[11] P. Dahlqvist and G. Russberg, Phys. Rev. Lett. **65**, 2837 (1990), and earlier references therein.
[12] A. Carnegie and I. C. Persival, J. Phys. A **17**, 801 (1984).